NeuroImage 285 (2024) 120472

Contents lists available at ScienceDirect

NeuroImage

journal homepage: www.elsevier.com/locate/ynimg

Activation network improves spatiotemporal modelling of human brain communication processes

Xucheng Liu [a,b], Ze Wang [c], Shun Liu [a,b], Lianggeng Gong [d], Pedro A. Valdes Sosa [e,f], Benjamin Becker [g,h], Tzyy-Ping Jung [i,j], Xi-jian Dai [a,b,d,*], Feng Wan [a,b,*]

[a] Department of Electrical and Computer Engineering, Faculty of Science and Technology, University of Macau, Macau 999078, China
[b] Centre for Cognitive and Brain Sciences, Institute of Collaborative Innovation, University of Macau, Macau, 999078, China
[c] Macao Centre for Mathematical Sciences, and the Respiratory Disease AI Laboratory on Epidemic Intelligence and Medical Big Data Instrument Applications, Faculty of Innovation Engineering, Macau University of Science and Technology, Macau, 999078, China
[d] Department of Radiology, The Second Affiliated Hospital of Nanchang University, Nanchang, 330006, China
[e] The Clinical Hospital of Chengdu Brain Sciences Institute. University of Electronic Sciences and Technology of China, Chengdu, 611731, China
[f] Cuban Neuroscience Center, La Habana 10200, Cuba
[g] State Key Laboratory of Brain and Cognitive Sciences, The University of Hong Kong, Hong Kong 999077, China
[h] Department of Psychology, The University of Hong Kong, Hong Kong 999077, China
[i] Department of Bioengineering, University of California at San Diego, La Jolla 92092, United States
[j] Swartz Center for Computational Neuroscience, Institute for Neural Computation, University of California at San Diego, La Jolla 92093, United States

ARTICLE INFO

Keywords:
Functional MRI
Dynamic functional network connectivity
Brain network
Topological analysis

ABSTRACT

Dynamic functional networks (DFN) have considerably advanced modelling of the brain communication processes. The prevailing implementation capitalizes on the system and network-level correlations between time series. However, this approach does not account for the continuous impact of non-dynamic dependencies within the statistical correlation, resulting in relatively stable connectivity patterns of DFN over time with limited sensitivity for communication dynamic between brain regions. Here, we propose an activation network framework based on the activity of functional connectivity (AFC) to extract new types of connectivity patterns during brain communication process. The AFC captures potential time-specific fluctuations associated with the brain communication processes by eliminating the non-dynamic dependency of the statistical correlation. In a simulation study, the positive correlation ($r = 0.966$, $p < 0.001$) between the extracted dynamic dependencies and the simulated "ground truth" validates the method's dynamic detection capability. Applying to autism spectrum disorders (ASD) and COVID-19 datasets, the proposed activation network extracts richer topological reorganization information, which is largely invisible to the DFN. Detailed, the activation network exhibits significant inter-regional connections between function-specific subnetworks and reconfigures more efficiently in the temporal dimension. Furthermore, the DFN fails to distinguish between patients and healthy controls. However, the proposed method reveals a significant decrease ($p < 0.05$) in brain information processing abilities in patients. Finally, combining two types of networks successfully classifies ASD (83.636 % ± 11.969 %, *mean* ± *std*) and COVID-19 (67.333 % ± 5.398 %). These findings suggest the proposed method could be a potential analytic framework for elucidating the neural mechanism of brain dynamics.

1. Introduction

The human brain establishes cognitive functions through continuous communication between multiple functional systems. Complex and multifaceted communication crucially supports efficient information processing. Numerous studies have utilized structural and functional brain networks to determine the neural mechanisms that allow efficient processing (Park and Friston, 2013; Sporns and Betzel, 2016; Buckner and DiNicola, 2019; Ricchi et al., 2022). Nevertheless, the relatively stable connectivity patterns over time poses a significant limitation of the functional network in modeling the brain's efficient communication process. The prevailing functional network approaches rely solely on

* Corresponding authors at: Department of Electrical and Computer Engineering, Faculty of Science and Technology, University of Macau, Macau 999078, China.
E-mail addresses: daixjdoctor@126.com (X.-j. Dai), fwan@um.edu.mo (F. Wan).

https://doi.org/10.1016/j.neuroimage.2023.120472
Received 28 June 2023; Received in revised form 8 November 2023; Accepted 22 November 2023
Available online 23 November 2023

statistical correlation and do not account for the complexity between the balance of dynamic neural fluctuations and essential maintenance. Therefore, capturing the precise dynamic neural fluctuations within statistical correlations and establishing an optimal spatiotemporal framework for brain communication remain significant challenges.

Efficient transmission or distribution of information requires coordinated engagement. In the context of brain networks, functional connectivity (FC) has been extensively utilized to characterize this process. Static FC is traditionally calculated using statistical correlations over the entire time series of data acquisition (Hutchison et al., 2013). Explorations of static FC on various physiological signals (EEG, EMG, fMRI, etc.) significantly extend our knowledge of the functional brain architecture underlying cognitive processes, diseases and their neural modulation (Petersen and Sporns, 2015; Ji et al., 2019; Zimmermann et al., 2018; Zhao et al., 2019; Xu et al., 2021; Wang et al., 2021). However, static FC ignores detailed moment-to-moment variations in the communication and thus cannot meet the advancing requirement of network neuroscience concerning inherent dynamics. Recently, the investigation of continuous neural interactions has attracted substantial interest. Among these studies, the sliding window is the most popular method for extracting moment-to-moment communications (Chang and Glover, 2010; Raut et al., 2021). Briefly, segmenting the entire time series into several shorter "windows" improves the statistical correlation's temporal resolution, and accounting for the windows can provide time-varying ("dynamic") FC (Sakoglu et al., 2010; Calhoun and Adali, 2016; Vidaurre et al., 2017; Zhou et al., 2020). The time-varying FC has been robustly associated with cognitive processes and changes in processing efficiency as a function of time-resolved communication trajectories within the given period (Zhang et al., 2016; Yang, 2023).

However, the conventional FC calculation largely relies on indirect measures, such that the time series indirectly encode information of neural activity that originates from a stream of spontaneous neural activity (Demertzi et al., 2019; Barttfeld et al., 2015; Laumann et al., 2017). This was demonstrated in studies using anesthesia, which showed that FC still fluctuates during unconsciousness, with some properties remaining similar to those of the conscious state (Amico et al., 2017; Vincent et al., 2007; Liang et al., 2015). Thus, a fraction of time-varying FC reflects non-cognitive intrinsic or homeostatic process (Lurie et al., 2020; Mostame et al., 2019). This non-cognitive component serves as the background during the communication process, making it essential to distinguish neural fluctuations precisely from the background. Therefore, a critical issue in characterizing communication is to develop a method that can sensitively detect the "ground truth" of neural communication processes underlying FC. Directly applying FC to measure the neural activity dynamics may not be optimal, as this approach fails to account for the underlying instantaneous dynamic dependency within the FC, thereby limiting quantification accuracy.

The functional network models brain activity and comprises statistical correlations between various functional systems. Depending on the static or time-varying FC application, the pattern of functional network is extended across spatial (static functional network, SFN) or spatiotemporal (dynamic functional network, DFN) scales. Regarding brain dynamics, the reconfiguration of DFN follows the evolution of the brain communication process. However, studies have highlighted the limitations of its organization. Anatomical structure strongly constrains the relationship between the brain's anatomical structure and functional network, as suggested by numerous studies (Honey et al., 2009; Hermundstad et al., 2013; Lu et al., 2011). Various anatomical elements and links are crucial for generating and propagating information flow in the human brain. This constraint contributes to the composition of task-irrelevant network patterns and compresses network alterations (Fox et al., 2005; De Luca et al., 2006; Lewisa et al., 2009). The connectivity pattern of DFN is relatively stable over time and similar to its group-averaged architecture (Mostame and Sadaghiani, 2021; Krienen et al., 2014). Such a stable pattern persists consistently across diverse tasks and brain functions (Cole et al., 2014). These findings suggest that the DFN is not sensitive to the communication dynamics of the human brain and provides little information on network reconfiguration during the brain communication process.

Current DFN construction methods directly apply pairwise statistical correlations to determine connections, allowing us to learn the distribution of joint functional activity between various brain regions and their temporal evolution (Farahani et al., 2019). However, this analytic framework is influenced by both neural activity and non-cognitive intrinsic or homeostatic processes, resulting in significant constraints in representing the brain communication process. Consequently, communication dynamics constitute only one aspect of DFN's topological properties. Especially, with the significant constraints, the DFN may be challenging to reconfigure its optimal topologies for complex information transmission modes to support one or more brain functions (Solé et al., 2002). From a natural selection perspective, directly using the DFN to characterize the brain communication processes is not economical concerning complex brain functions. We must consider an alternative network to describe the brain communication processes precisely. The underlying instantaneous dynamic dependency within the FC could be a valuable marker to assess the dynamic of the communication process. As a result, a new framework is required to model the dynamic communication extracted from DFN.

This work proposes a novel framework called an activation network to more accurately capture the underlying spatiotemporal reorganization within the dynamic functional network. To address the limitations of the current DFN framework for detecting dynamics due to background dependency within FC, we assume that the activity of functional connectivity (AFC) and background of functional connectivity (BFC) represent FC's communication dynamics and non-dynamic dependencies, respectively. The BFC is the non-dynamic dependency within the statistical correlation, calculated based on the time-invariant properties of time series from pair-wise brain regions. The AFC eliminates the non-dynamic dependencies of the statistical correlation to capture potential time-specific fluctuations associated with the brain communication processes, thereby characterizing dynamic dependencies. We then compose the activation network to extract the spatiotemporal patterns of the communication processes based on the AFC. The simulation validates the dynamic detection ability of AFC, proving its sensitivity to predefined dynamics. Applying the framework to resting-state fMRI datasets we demonstrate that the proposed method can efficiently extract inter-regional connections between function-specific systems and establish a more comprehensive description of topological reorganization. The proposed method is also validated by its application to classifying individuals with autism spectrum disorders (ASD) and coronavirus disease infections (COVID-19). It can also work with DFN to provide a more comprehensive description of the brain communication process. The activation network establishes an appropriate spatiotemporal framework to characterize the communication processes underlying dynamic brain activity.

2. Materials and methods

Fig. 1 depicts a schematic presentation of the AFC approach and establishing the activation network. In the pairwise time series and sliding window method, the primary problem is recognizing time-invariant and time-specific properties of time series during brain communication. The whole time series retains the general (time-invariant) properties shared across different time windows. For windowed time series, it follows both time-invariant evolutionary rules and time-specific properties because of the communication dynamics of brain activity. The windowed correlation is computed by directly applying Pearson's correlation to the windowed time series. Additionally, we assume there is no brain dynamic within the time series. The background of functional connectivity (BFC) within each window is computed by introducing the time-invariant properties from whole time series into windowed time series while correlation calculation. The

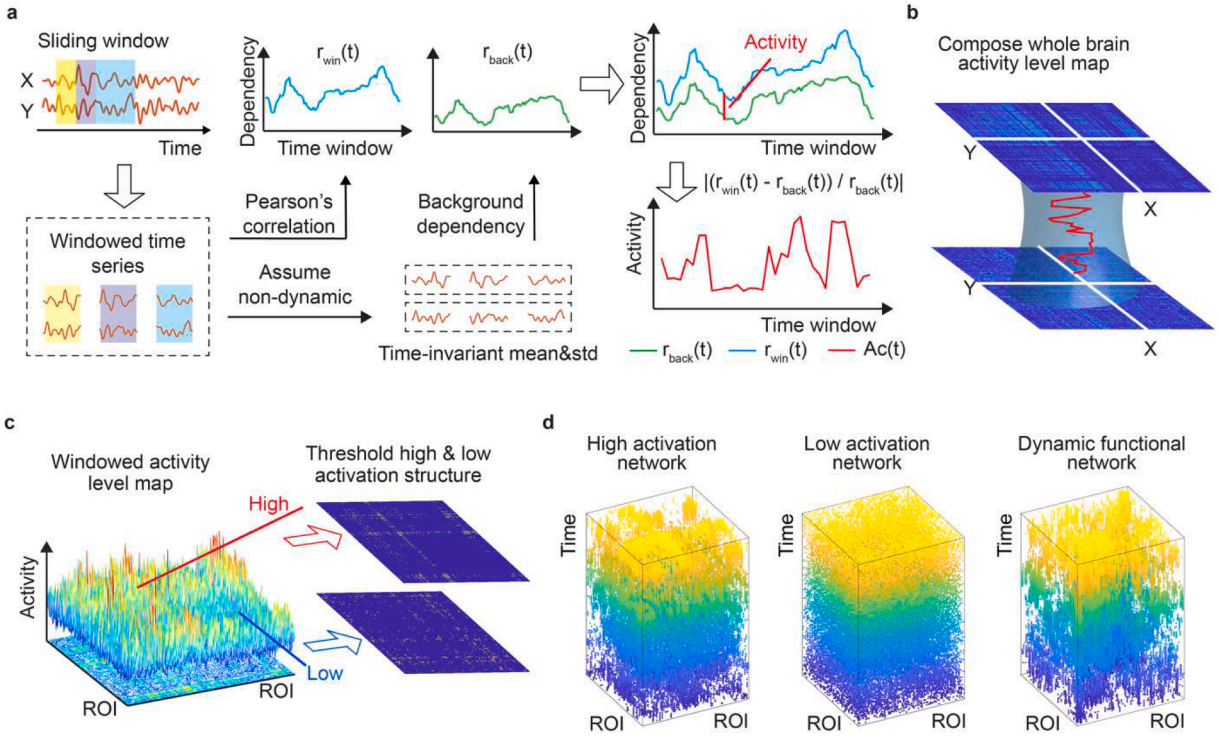

Fig. 1. The overview of extracting AFC and establishing the activation network. (a) The AFC calculation process. Time series from two arbitrary regions (X and Y) in the human brain are used to calculate the AFC between any two regions of interest (ROIs). With the pairwise time series and sliding window method, the primary problem is recognizing time-invariant and time-specific properties of time series during brain communication. The whole time series retains the general (time-invariant) properties shared across different time windows. The windowed time series emphasizes the property of a limited period, encompassing both time-invariant evolutionary rules and time-specific fluctuations resulting from the communication dynamics of brain activity. The windowed correlation is computed by directly applying Pearson's correlation to the windowed time series. Additionally, we assume there is no brain dynamic within the time series. The background of functional connectivity (BFC) within each window is computed by introducing the time-invariant properties from the whole time series into the windowed time series while correlation calculation. The activity of functional connectivity (AFC) is computed by the relative difference between windowed correlation and BFC. **(b)** The whole brain activity level map comprises the AFC between all ROIs. **(c)** Each windowed activity level map could be thresholded according to two opposite activity levels to extract high and low activation structures. The high activation structure shows the connections activated at this time, while the low activation structure shows the relatively stable connections. **(d)** Examples of the high activation network (HAN), low activation network (LAN), and dynamic functional network (DFN). They are from a randomly selected subject of the healthy controls of the ASD dataset. $r_{win}(t)$: windowed correlation at time window t. $r_{back}(t)$: BFC at time window t. $Ac(t)$: AFC at time window t.

activity of functional connectivity (AFC) is computed by the relative difference between windowed correlation and BFC. We defined the BFC as the dependency within windowed correlation computed based on the time-invariant properties. We defined the AFC as the dependency within windowed correlation that encompasses time-specific properties after removing its corresponding background. The AFC measures the extent to which the activity level of statistical correlation is activated from the general state to the time-specific state. Then, AFC across all regions of interest (ROIs) is used to construct the map of the whole brain activity level. The opposite activity levels could extract two different high and low activation patterns for each time window. Thus, the spatiotemporal connectivity pattern of the activation network includes a high activation network (HAN) and a low activation network (LAN).

2.1. Activation network

2.1.1. Activity of functional connectivity calculation

Statistical correlation can be expressed in various ways, such as coherence, phase synchronization, mutual information, etc. Pearson's correlation calculates the linear correlation between pairwise time series and is the most common and simplest method (Farahani et al., 2019). Therefore, it was chosen as an example to show the computation of the activity of functional connectivity in this study.

We start with pairwise discrete non-stationary time series $X = \{x_i\}_{i=1,2,\ldots,n}$ and $Y = \{y_i\}_{i=1,2,\ldots,n}$. We apply a sliding-window method with a window length of w and a step length of s to segment windowed time series, denoted as x_t and y_t, at the tth time window from the whole time series X and Y. Pearson's correlation of the windowed time series x_t and y_t is:

$$r(t) = \frac{\sum_{i=1}^{w}(x_{i,t} - \bar{x}_t)(y_{i,t} - \bar{y}_t)}{w\sigma_{x_t}\sigma_{y_t}} \quad (1)$$

where $x_{i,t}$ and $y_{i,t}$ are the ith time points within tth time window and w is the number of time points within the time window, and $\bar{x}_t$ and $\bar{y}_t$ are denoted as the means of x_t and y_t, and σ_{x_t} and σ_{y_t} are denoted as the standard deviations of x_t and y_t.

As the brain activity is dynamic, the time series across time windows do not follow the second-order stationary assumption where their distribution is not constant. The means and standard deviations of windowed time series x_t and y_t are $\bar{x}_t = \frac{1}{w}\sum_{i=1}^{w}x_{i,t}$, $\bar{y}_t = \frac{1}{w}\sum_{i=1}^{w}y_{i,t}$, $\sigma_{x_t} = \sqrt{\frac{1}{w}\sum_{i=1}^{w}(x_{i,t} - \bar{x}_t)^2}$, $\sigma_{y_t} = \sqrt{\frac{1}{w}\sum_{i=1}^{w}(y_{i,t} - \bar{y}_t)^2}$. Therefore, the windowed correlation $r_{win}(t)$ at time window t is calculated by:

$$r_{win}(t) = \frac{\sum_{i=1}^{w}x_{i,t}y_{i,t} - w\bar{x}_t\bar{y}_t}{\sqrt{\sum_{i=1}^{w}x_{i,t}^2 - w\bar{x}_t^2}\sqrt{\sum_{i=1}^{w}y_{i,t}^2 - w\bar{y}_t^2}} \quad (2)$$

The background of functional connectivity $r_{back}(t)$ at time window t is calculated based on the time-invariant properties. If we assume there is no brain dynamic, the windowed time series x_t and y_t follow the time-

invariant distribution that consistent with the whole time series X and Y. In this case, the $r_{back}(t)$ at time window t is calculated based on assuming a time-invariant means and standard deviations of the whole time series X and Y: $\bar{x}_t = \bar{x},\ \bar{y}_t = \bar{y},\ \sigma_{x_t} = \sigma_x,\ \sigma_{y_t} = \sigma_y$, where $\bar{x}$ and $\bar{y}$ are denoted as the means of X and Y, and σ_x and σ_y are denoted as the standard deviations of X and Y. If we normalize the whole time series X and Y such that $\bar{x} = 0,\ \bar{y} = 0,\ \sigma_x = 1, \sigma_y = 1$, the $r_{back}(t)$ is calculated by:

$$r_{back}(t) = \frac{1}{w}\sum_{i=1}^{w} x_{i,t}y_{i,t} \tag{3}$$

The activity of functional connectivity $Ac(t)$ at time window t is calculated by subtracting the background component from the windowed correlation. However, since the $r_{back}(t)$ is not constant across time windows, simply the difference between $r_{win}(t)$ and $r_{back}(t)$ cannot be directly compared between different time windows. Therefore, the $Ac(t)$ is calculated by the relative difference between $r_{win}(t)$ and $r_{back}(t)$ at time window t:

$$Ac(t) = \left|\frac{r_{win}(t) - r_{back}(t)}{r_{back}(t)}\right| \tag{4}$$

The AFC measures the extent to which the activity level of statistical correlation is activated from the general state to the time-specific state. Specifically, when no difference between windowed correlation and its background ($r_{win}(t) = r_{back}(t)$) at time t, the value of $Ac(t)$ is 0 that there is no brain dynamic. On the other hand, the larger difference between $r_{win}(t)$ and $r_{back}(t)$, the greater the value of $Ac(t)$, indicating the activity of functional connectivity is more activated from the background state at time t and a higher level of brain dynamic.

2.1.2. High and low activation network construction

The activation network uses the AFC between various functional systems to model brain activity. It is a spatiotemporal network (node * node * time) represented as sets of nodes and their pairwise connections, where the nodes are ROIs, and the values of AFC measure the connections. This approach allows for studying the distribution of connections activated at different levels of brain activity and their temporal evolution. The activation network measures the underlying activity of the functional structure (DFN). Considering high and low activity levels, sets of the connections with the highest and lowest AFC values are used to construct the high activation network (HAN) and low activation network (LAN) to represent different modes during the communication process. The HAN is a spatiotemporal network encompassing connections from each time window with the highest AFC values. It indicates the highly dynamic spatiotemporal connectivity pattern that emerges during brain communication. The LAN is a spatiotemporal network encompassing connections from each time window with the lowest AFC values. It indicates the low dynamic spatiotemporal connectivity pattern that emerges during brain communication. We use both HAN and LAN in the following analysis. Table 1 provides a brief glossary of terms used in this article.

2.2. Datasets

2.2.1. Simulated resting-state BOLD-fMRI data

Using simulated resting-state BOLD-fMRI data, we can control the time series' "ground truth". This allows us to simulate functional connectivity's activity and background properties to assess the proposed method's dynamic detection ability. To do this, we measure the level of strengthening and weakening of background correlation influenced by dynamic (ΔFC) to express the activity of functional connectivity. Simulated BOLD-fMRI is generated by a multivariate Gaussian process and a first-order Vector Autoregressive (VAR) model to simulate the background and dynamic data (Supplementary Fig. 1), respectively (Thompson et al., 2018). The background data mainly provide the stability of FC.

Table 1
Glossary of terms used in this article.

Name	Measurement and meaning	Index
Windowed correlation	The statistical correlation among the windowed pairwise neurophysiological time series derived from various brain regions. It is assumed to retain both dynamic and non-dynamic dependencies due to the communication dynamics and non-cognitive intrinsic or homeostatic processes of brain activity.	Fig. 1a
Background of functional connectivity (BFC)	The dependency within windowed correlation computed based on the time-invariant properties.	Fig. 1a
Activity of functional connectivity (AFC)	The dependency within windowed correlation that encompasses time-specific properties after removing its corresponding background. It measures the extent to which the activity level of statistical correlation is activated from the general state to the time-specific state.	Fig. 1a
High activation network (HAN)	The spatiotemporal network encompassing connections from each time window with the highest AFC values. It indicates the highly dynamic spatiotemporal connectivity pattern that emerges during brain communication.	Fig. 1d
Low activation network (LAN)	The spatiotemporal network encompassing connections from each time window with the lowest AFC values. It indicates the low dynamic spatiotemporal connectivity pattern that emerges during brain communication.	Fig. 1d
Time-varying functional connectivity (time-varying FC)	Segmenting the entire time series into several shorter "windows" improves statistical correlation's temporal resolution, and accounting for the windows can provide time-varying FC.	Section 1
ΔFC	The level of strengthening and weakening of background correlation influenced by dynamic to express the activity of functional connectivity. It is applied to quantify the dynamics of simulated BOLD-fMRI data.	Section 2.2.1

To generate the background data, we use pairwise zero-mean multivariate Gaussian processes, $\sigma = (\sigma_1, \ldots, \sigma_n)$, with a randomly generated covariance matrix Σ between -1 and 1 to represent background correlation. We then specify the dynamics of the simulated data. We expect the background correlation to be influenced stochastically by dynamics to reflect the ongoing nature of resting-state BOLD-fMRI fluctuations. The dynamic data are estimated pairwise from the first-order VAR model: $\varepsilon_t = A\varepsilon_{t-1} + e_t$, where $A = 0.8$ is the autocorrelation coefficient, and e_t is the residual of the model determined by random Gaussian process with a mean of 0.2 and standard deviation (std) of 0.12 (Supplementary Fig. 2). Finally, the simulated BOLD-fMRI data are the linear combination of background and dynamic data: $V = \sigma + \varepsilon_t$. We validate the proposed method by correlating it withΔFC. We generate data 5000 times with a data length of 3000 points to ensure reliable output.

2.2.2. Autism spectrum disorders (ASD) data

The ASD data used in this study are obtained from the Autism Brain Imaging Data Exchange (ABIDE) (Di Martino et al., 2014). To exclude the influence of multiple recording sites, we have opted to choose a single site for our study, employing two specific criteria for selection: 1) Sufficient subject number; 2) Sufficient data length. The resting-state fMRI data of children from the University of Michigan (sample 1) site meets these criteria most effectively. The data includes 110 participants, of which 55 are patients with ASD (12.73 ± 2.45 years; 83.64 % male) and the remaining are healthy controls (14.07 ± 3.18 years; 69.09 %

male). The resting-state fMRI data are acquired using a 3 Tesla GE Signa scanner. Resting-state fMRI data are recorded with an EPI sequence (TR 2 s, TE 30 ms, flip angle 90°, spatial resolution 3.4 * 3.4 * 3.0 mm) during a 10-minute eyes-open scan. All images are obtained with informed consent following established human participant research procedures. Detailed information can be found at http://fcon_1000.projects.nitrc.org/indi/abide/.

2.2.3. COVID-19 data

The UK Biobank has been gradually releasing resting-state functional magnetic resonance imaging data from the COVID-19 re-imaging research, with a total of 490 functional volumes recorded using a single-shot gradient recalled echo–planar imaging pulse sequence (Sudlow et al., 2015). As of 31 May 2022, 613 adult participants below 65 met the inclusion criteria. Out of these, 299 adult participants (43.81 % men; aged 59.48 ± 3.58 years) were found to have been infected with SARS-CoV-2 based on their primary care (GP) data, hospital records, diagnostic antigen test results identified through record linkage to the Public Health datasets in England, Wales and Scotland, or two concordant antibody-based home lateral flow kit positive results. Three hundred fourteen adult participants (44.90 % men; aged 59.43 ± 3.48 years) were healthy controls. The resting-state fMRI data are acquired using a 3 Tesla Siemens Skyra scanner. Resting-state fMRI data are recorded with an EPI sequence (TR 735 ms, TE 39 ms, flip angle 52°, spatial resolution 2.4 * 2.4 * 2.4 mm). Each participant underwent a six minute, eyes-open acquisition. All images are obtained with informed consent, following established human participant research procedures. The follow-up data of 613 participants are included in this study. Detailed information is found at https://www.ukbiobank.ac.uk.

2.3. Data pre-processing

The resting-state functional volumes underwent data pre-processing using the Data Processing & Analysis for Brain Imaging (DPABI) v3.1 toolbox (http://rfmri.org/DPABI) toolbox, which involved form transformation, slice timing, head motion correction, spatial normalization to the Montreal Neurological Institute (MNI) space at a re-sampling resolution of $3 \times 3 \times 3$ mm^3 spatial smoothing ($6 \times 6 \times 6$mm^3 full width at half maximum), linear detrending to reduce low-frequency drift and physiological high-frequency respiratory and cardiac noise, and temporally bandpass filtered (0.01–0.1 Hz). The Friston 24-parameter model was used to regress out head motion effects. A participant with $\geq$ 1.5 *mm* maximum translation in *x*, *y*, or *z* directions and/or $\geq 1.5^\circ$ of motion rotation was removed. Linear regression was applied to remove the global mean signal, white matter, and cerebrospinal fluid signal. The registered fMRI volumes were partitioned using the Dosenbach 160 ROIs template.

2.4. Network construction

We used a sliding window approach with a window length of 30 TRs and a step length of 3 TRs to ensure a good temporal resolution of AFC while maintaining statistical reliability, as indicated in Supplementary Table 1–3. The resulting AFC values were then used to construct the activation network. To build the HAN and LAN, we applied sparsities of 10 % (ASD) and 25 % (COVID-19) to each slide of the activation network to include connections with top or bottom activation values. We also used time-varying FC to construct the DFN for comparison and applied the same sparsities to the corresponding dataset.

2.5. Graph theoretical analysis

Graph theory provides a mathematical framework to measure the complex topology of the brain network quantitatively. Both the obtained adjacent matrices (activation network and DFN) are binarized to represent the existence or nonexistence of connections. We use graph theory to evaluate the topological reorganization of networks. Detailed, the mean clustering coefficient (*C*), characteristic path length (*L*), local efficiency (*El*), and global efficiency (*Eg*) are used as the parameters of spatial topology (Bullmore and Sporns, 2009). Meanwhile, *C* and *El* measure the information transmission ability on a local scale, and *L* and *Eg* measure the information transmission ability on a global scale. All of them are measurements of brain functions of local segregation and global integration.

2.6. Classification

The ASD and COVID-19 datasets are classified based on cross-subject graph properties (*C*, *L*, *El*, *Eg*) extracted from HAN, LAN, and DFN. We extract graph properties from each time window and mix them for each subject to achieve cross-subject classification. We compared the classification performances of three groups: activation network (HAN and LAN), DFN, and their combination. To ensure robust evaluation, we employ a 10-fold cross-validation approach within each group to split training and testing data. In order to prevent information leakage between the training and testing data during the classification process, we strictly perform feature selection exclusively on the training data within each fold of the cross-validation process. First, we included the top 100 features based on the first 100 different mean values among the different classes within the training data. Secondly, we evaluated the importance of each feature using the F value and composed the feature subsets of these features. The feature subsets are formed by progressively selecting 1 to 100 features according to their importance, resulting in 100 distinct subsets with varying numbers of features. Then, a preliminary classification is conducted solely on the training data by a support vector machine (SVM) to determine the most important feature subset. We then applied the selected features from the training data to the testing data using the feature indices derived from the feature selection to ensure consistency between them. After feature selection, four mainstream classification strategies are used, including support vector machine (SVM), random forest (RF), Adaboost, and naive Bayes (NB). We applied the linear kernel in SVM and used sequential minimal optimization (SMO) as the learning method. The best c is selected by cross-validation in the parameter space of $10^{-4}, \ldots, 10^{-1}$.

2.7. Statistical testing

Paired *t*-test is applied to compare the difference between time-varying FC and background correlation, as well as AFC and ΔFC. An independent *t*-test is applied to compare the temporal similarity of network between the activation network and DFN, respectively. Furthermore, to show the different temporal reorganization processes of different network, the independent *t*-test is applied to compare graph parameters (*C* and *L*) between HAN, LAN, and DFN, respectively. We measured the redundancy of network communication efficiency by lesioning the network and removing inter- or intra-regional connections. We then used an independent *t*-test to compare the damage levels calculated by *C* and *L* on the HAN, LAN, and DFN. To select the most sensitive network to mental state alteration, we calculated the graph parameters (*C*, *L*, *El*, and *Eg*) of HAN, LAN, and DFN for each. We used an independent *t*-test to compare the difference in graph parameters between patients and healthy controls datasets. We employed a significance level of $p < 0.05$ and applied correction for multiple comparisons with the false discovery rate (FDR) at $q = 0.05$. All p-values were calculated as two-tailed p-values.

3. Results

3.1. Dynamic detection ability of AFC and FC

We apply the AFC method to simulated resting-state BOLD-fMRI data

to validate its performance with known "ground truth". As BOLD-fMRI signals record neural fluctuations based on spontaneous activity, we use simulated dynamic and background data to simulate this process. The window and step lengths are set to 30 and 30 points, respectively. We measure the dynamic of functional connectivity by the change level in background correlation (ΔFC) after combining dynamic data with background data. The performance of the proposed method is then validated by correlating it with ΔFC.

Fig. 2a reflects that FC is highly correlated ($r = 1, p = 0.950$) with the background correlation across 5000 samples. Fig. 2b depicts a randomly selected sample to facilitate illustration. These results suggest that FC is more indicative of the background correlation than the dynamic correlation and that the trajectory of time-varying FC is largely influenced by components that provide the dominant dependencies (Supplementary Fig. 2). Thus, FC may not be suitable for directly detecting neural dynamics. We then calculate AFC and ΔFC to validate the proposed method's communication dynamic detection ability. Results show that AFC exhibits a significant difference with ΔFC ($t_{4999} = 127.674$, $p < 0.001$; Fig. 2c). However, Fig. 2d also demonstrates a significant positive correlation ($r = 0.966$, $p < 0.001$) between them, indicating that the proposed AFC is sensitive to dynamic fluctuations under the influence of background correlation. Furthermore, these findings suggest that AFC is applicable for constructing the dynamic communication of the human brain.

3.2. The activation network describes richer network variation and different reorganization modes than DFN in the time domain

We applied the proposed method to two distinct resting-state fMRI datasets (ASD and COVID-19), which involve different populations and data recording settings. This utilization of diverse datasets aims to demonstrate the robustness, reliability, and replicability of the proposed method. Specifically, we applied AFC and time-varying FC to resting-state fMRI data to construct the activation network and DFN. The communication patterns in the human brain result in a complex process of network reorganization. A dynamic network should capture rich information about network reorganization within the entire time series. To evaluate this, we compared the spatial correlation between temporal averaged and windowed fully connected matrices for each participant. A lower correlation indicates greater network variation over time, which suggests richer information about topological reorganization. Graph parameters of clustering coefficient (C) and characteristic path length (L) are applied to quantitatively evaluate the spatial topology of the network within each time window. The healthy controls from the two datasets are selected for analysis, respectively. For each dataset, the distributions of graph properties across selected participants and time windows indicate unique temporal reorganization processes of each network. The temporal evolutions of different network topologies are evaluated in the aspects of local segregation and global integration.

First, AFC matrices provide more information on network variations than DFN during the communication processes of the human brain. The windowed AFC matrices show significantly lower averaged correlations (ASD: $t_{108} = -66.106$, $p < 0.001$, COVID-19: $t_{626} = -84.604$, $p < 0.001$) with their temporal averaged matrices (Fig. 3a,f; Supplementary Figs. 3, 4). In contrast, the connectivity pattern of DFN is relatively stable over time, consistent with the results of previous studies (Mostame and Sadaghiani, 2021; Krienen et al., 2014). Therefore, the extracted activation network from AFC presents a richer variation of network pattern over time, with a higher potential for extracting the communication dynamic of brain activity. Secondly, as shown in Fig. 3b, c,g and h, HAN, LAN, and DFN show different distributions of graph parameters, suggesting a unique evolution process for each network during the same period (Supplementary Fig. 5–8). Specifically, Fig. 3d,e, i and j show that the topologies of HAN, LAN, and DFN differ in their local segregation and global integration functions, where graph parameters of C and L significantly differ ($p < 0.001$, $FDR-corrected$). These outcomes imply distinct topological organization modes of the activation network and DFN during communication (Fig. 1d). In summary, the activation network describes richer connectivity pattern variations of the brain network, exhibiting a different reorganization mode in the time domain compared to DFN. However, to better understand the spatiotemporal properties of the activation network, we need to analyze its details and validate the reliability of the provided information by the activation network.

3.3. The activation network focuses on inter-regional connections of function-specific subnetworks

Temporal averaged networks of the activation network and DFN are calculated to present their connectivity patterns in the spatial dimension. Healthy controls from both datasets are selected. HAN, LAN, and DFN are averaged over time windows and participants. To better illustrate the connectivity pattern, we summarize the proportion of connections located in the six specific subnetworks, namely the Cingulo-opercular network (CON), Sensorimotor network (SMN), Occipital network (ON), Fronto-parietal network (FPN), Default mode network (DMN), and Cerebellum network (CN).

As shown in Fig. 4, spatial distributions between HAN, LAN, and DFN differ. HAN and LAN are related to function-specific subnetworks: HAN connections are primarily related to SMN (ASD: 11.635 %; COVID-19:

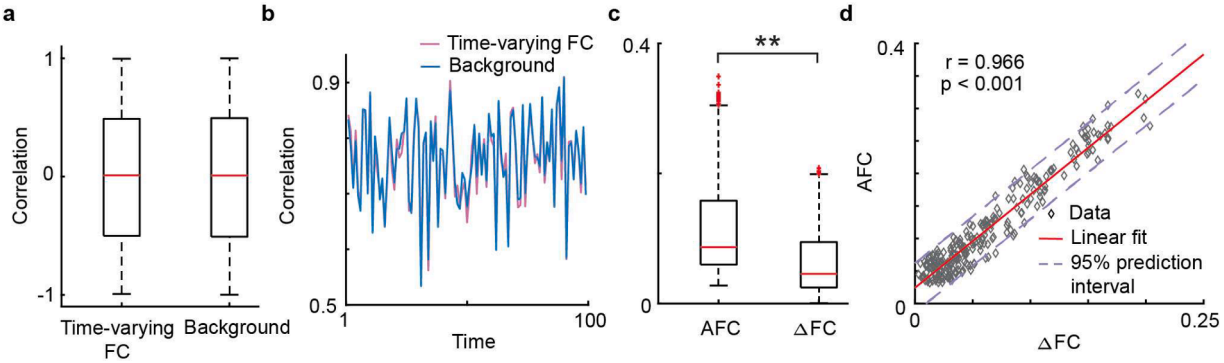

Fig. 2. The validation of the dynamic detection power of FC and AFC. (a) A box plot of time-varying FC and background correlation across 5000 samples. Time-varying FC does not differ significantly from background correlation. **(b)** Example of time-varying FC and background correlation. It is randomly selected from 5000 samples. These results suggest the time-varying FC trajectory highly relates to background correlation, which provides dominant correlations to obscure the underlying dynamic information. **(c)** A box plot of AFC, and ΔFC across 5000 samples. AFC and ΔFC are significantly different. **(d)** A scatter plot of AFC and ΔFC. They show a significant positive correlation with each other, indicating the high dynamic detection power of AFC. ΔFC refers to the strengthening and weakening level of the background correlation influenced by dynamic. **: $p < 0.001$.

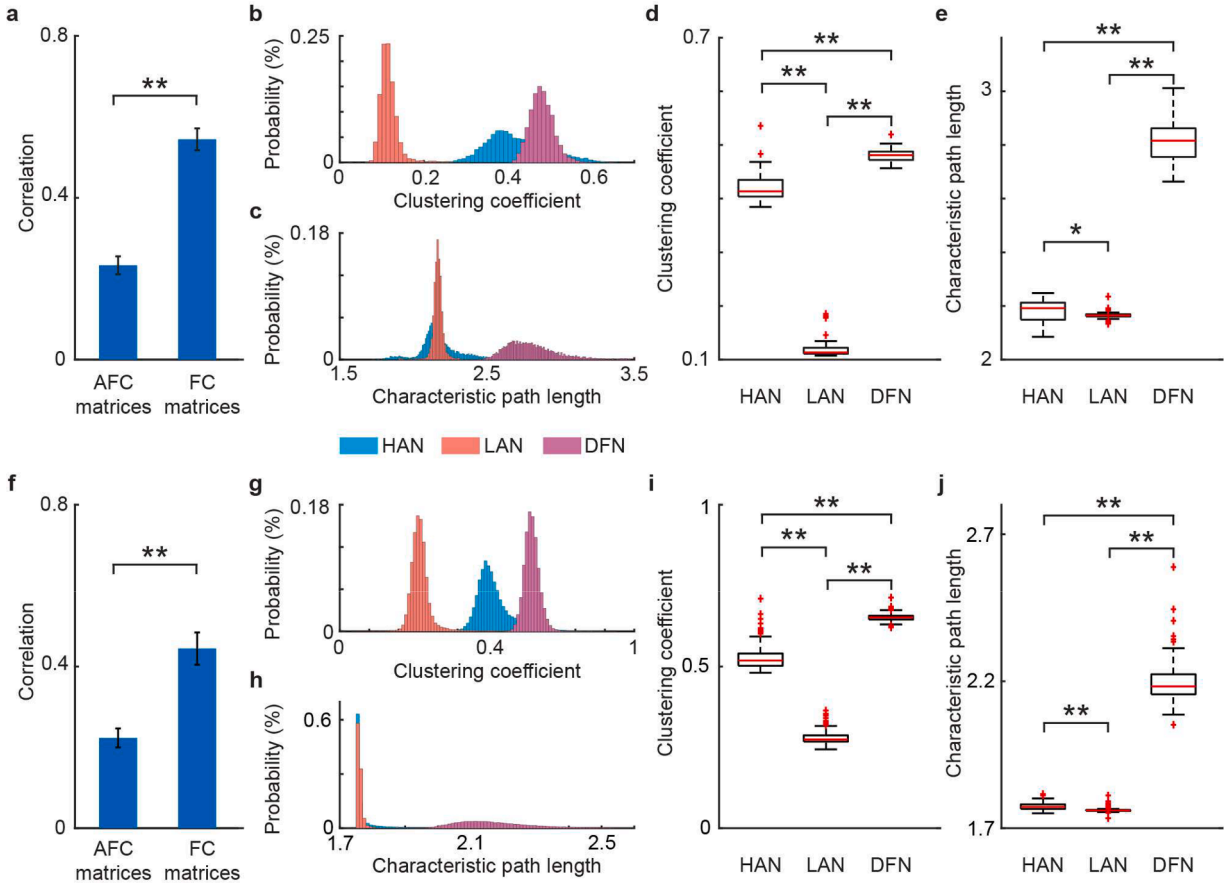

Fig. 3. Temporal reorganization of activation network in ASD (top panels) and COVID-19 (Bottom panels). (a, f) The temporal similarity of AFC and FC matrices in **(a)** ASD and **(f)** COVID-19. To evaluate the similarity of each participant's network, we compare the spatial correlation between temporal averaged and windowed fully connected matrices. The AFC matrices exhibit greater variability in the time domain and a higher potential to capture the communication dynamics of brain activity. **(b, c, g, h)** Probability distributions of graph parameters of HAN, LAN, and DFN in **(b, c)** ASD and **(g, h)** COVID-19. Graph parameters (C and L) are calculated from each time window to represent network topology at one-time step. Mixed graph parameters across participants indicate the temporal reorganization processes of corresponding networks. **(d, e, i, j)** Box plot of graph parameters of HAN, LAN, and DFN in **(d, e)** ASD and **(i, j)** COVID-19. Combined with their probability distributions, HAN, LAN, and DFN shows a significant difference in temporal reorganization and network topology. Noteworthy, the activation network and DFN are extracted to describe different aspects of brain activity. Every aspect includes critical information. Therefore, their graph parameters are not directly comparable to suggest which is better, and the statistical results indicate the significant difference. *: $p < 0.05$; **: $p < 0.001$, $FDR - corrected$.

6.761 %), whereas LAN connections are mostly related to DMN (ASD: 16.981 %; COVID-19: 12.107 %) indicating that a high proportion of connections are located within these regions (Supplementary Fig. 9, 10). In contrast, DFN adheres stronger to the predefined structure of the human brain that shows a balanced connection distribution of each subnetwork (Fig. 4c and g). Furthermore, the significant subnetworks of HAN and LAN tend to communicate with other regions that there is a high proportion of connections between SMN in HAN (ASD: 24.175 %; COVID-19: 30.236 %) and DMN in LAN (ASD: 25.590 %; COVID-19: 15.739 %) to other regions. Additionally, as shown in Fig. 4d and h, significant inter-regional connections are included in HAN (ASD: 79.874 %; COVID-19: 92.233 %) and LAN (ASD: 74.057 %; COVID-19: 64.780 %). Conversely, DFN does not include sufficient inter-regional connections (ASD: 29.088 %; COVID-19: 51.258 %). It suggests the activation network and DFN are distinct architecture that focus on opposite communication modes (inter- or intra-regional communication) of the brain network.

3.4. The connectivity pattern of the activation network is efficient and economical to achieve its reorganization in the time domain

We evaluate the connectivity patterns of HAN, LAN, and DFN in the spatial dimension concerning natural selection criteria: stable communication efficiency and low wiring cost. To assess communication efficiency, we simulate damage to the network's connections by respectively removing inter-regional and intra-regional connections to determine the impact on communication efficiency (Supplementary Fig. 11). We use graph parameters (C and L) from the non-damaged network as the baseline and calculate the damage level of each graph parameter. The healthy controls from two datasets are selected for analysis.

As shown in Fig. 5, only removing inter-regional connections causes more significant damages on C ($p < 0.001$, $FDR - corrected$) in both HAN and LAN, suggesting a significant impact on the brain function of local segregation. However, the connectivity pattern of DFN has low redundancy of damage as removing inter-regional connections significantly influences L ($p < 0.001$, $FDR - corrected$) and removing intra-regional connections shows significant impacts on both C and L ($p < 0.001$, $FDR - corrected$). This indicates a relatively high redundancy of the activation network connectivity pattern, which could maintain a relatively stable communication efficiency during its reorganization. Furthermore, it shows the importance of inter-regional connections in the activation network, as removing more inter-regional connections causes greater damage to C (ASD: $r = 0.556$, $p < 0.001$; COVID-19: $r = 0.643$, $p < 0.001$). Nevertheless, results in the DFN highlight the importance of intra-regional connections. On the one hand, damages on L are negative correlation (ASD: $r = -0.795$, $p < 0.001$; COVID-19: $r = -0.527$, $p < 0.001$) to the

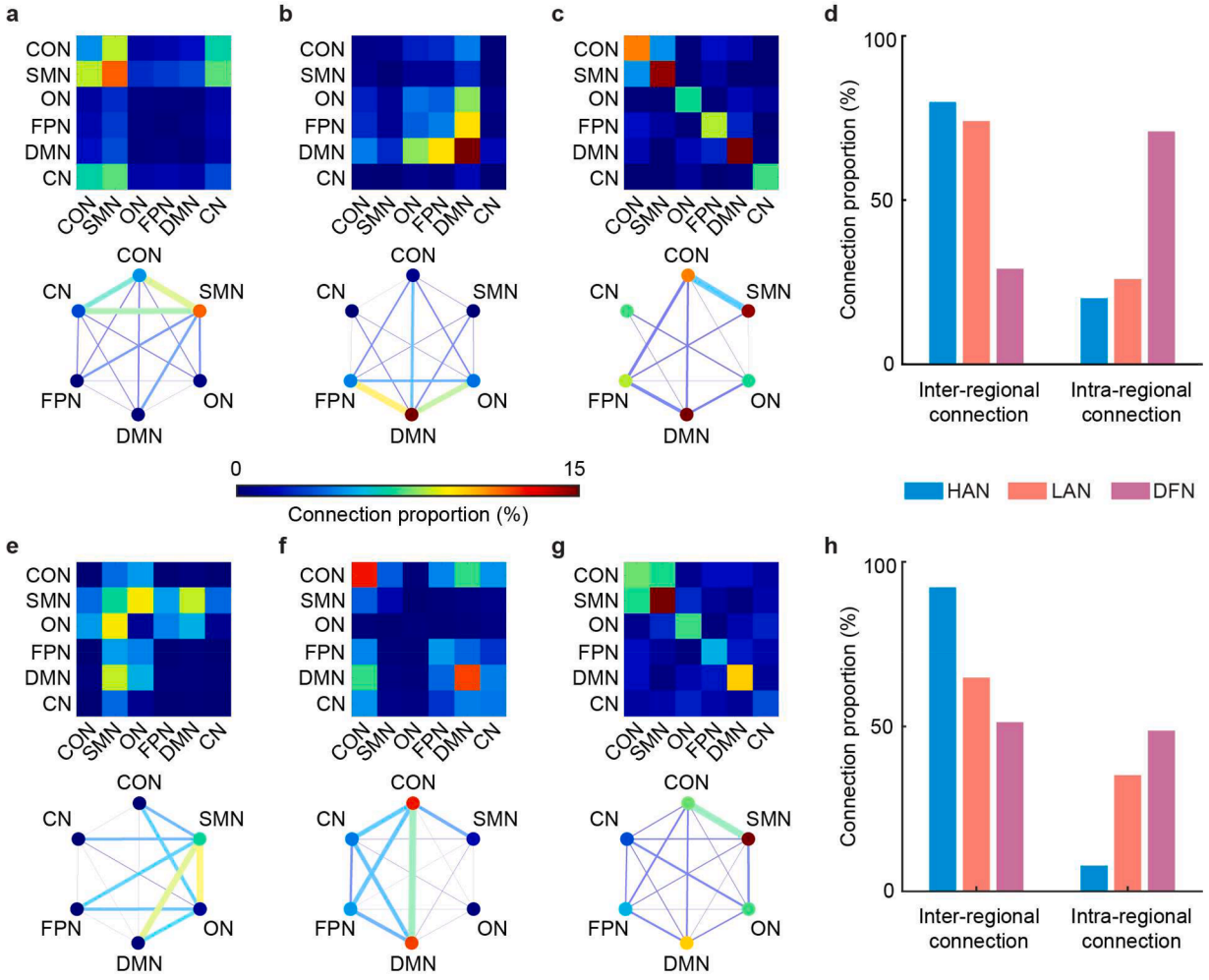

Fig. 4. Averaged network of HAN, LAN, and DFN and their connection distributions in ASD (top panels) and COVID-19 (bottom panels). The networks are averaged across all participants from healthy controls of each dataset. **(a-c, e-g)** The connection distributions of HAN, LAN, and DFN, which are the percentages of connections located intra- or inter-subnetworks with total connections. HAN and LAN are related to function-specific subnetworks, with HAN connections mostly related to SMN and LAN connections mostly related to DMN. However, DFN is more about the predefined structure of the human brain, showing a balanced connection distribution of each subnetwork. Particularly, HAN and LAN tend to communicate with other regions. **(d, h)** the proportions of inter- and intra-regional connections. It suggests the activation network and DFN are distinct architecture, focusing on the opposite communication modes (inter- or intra-regional communication). CON: Cingulo-opercular network, SMN: Sensorimotor network, ON: Occipital network, FPN: Fronto-parietal network, DMN: Default mode network, and CN: Cerebellum network. The color bar serves to represent the proportion of existing connections to the total potential connections within each subnetwork.

proportion of inter-regional connections be removed. On the other hand, damages on both C and L are positive correlation (C: ASD: $r = 0.775$, $p < 0.001$; COVID-19: $r = 0.758$, $p < 0.001$; L: ASD: $r = 0.447$, $p < 0.001$; COVID-19: $r = 0.494$, $p < 0.001$) to the proportion of intra-regional connections be removed. It suggests that the activation network and DFN focus on the different aspects of the communication processes by focusing on inter- and intra-regional connections. Meanwhile, simulation results prove fluctuation of FC is significantly constrained by background correlation (Fig. 2a and b). The change of DNF's connection must overcome the impact of background correlation with higher cost. The experimental results suggest that its network exhibits a high temporal correlation in the real condition (Fig. 3a and f) and prove its connectivity pattern is stable while maintaining stable communication efficiency. Therefore, the connectivity pattern described by the activation network has a relatively low wiring cost and stable communication efficiency to achieve its temporal evolution.

3.5. HAN and LAN play different roles in the activation network

The advantage of the activation network in the spatiotemporal domain has been presented previously. However, the correlation between HAN and LAN remains unclear. According to the activity level, the activation network segments two different connectivity patterns with opposite high and low activity, significantly different from DFN. As shown in Fig. 3, HAN and LAN display different distributions of graph parameters during the brain communication process. Specifically, HAN exhibits significantly higher C (ASD: $t_{108} = 71.980$, $p < 0.001$, COVID-19: $t_{626} = 113.866$, $p < 0.001$, $FDR - corrected$) and L (ASD: $t_{108} = 2.588$, $p = 0.011$, COVID-19: $t_{626} = 18.608$, $p < 0.001$, $FDR - corrected$) than LAN, indicating different reorganization modes during communication. Furthermore, Fig. 4 shows that HAN and LAN separately correlate to some function-specific subnetworks, and their combination creates a comprehensive map of the brain network. These findings show that HAN and LAN have distinct topological reorganization processes that coordinate to display activities of various functional systems during the communication process. Therefore, both HAN and LAN are critical for analyzing the communication dynamics of the human brain.

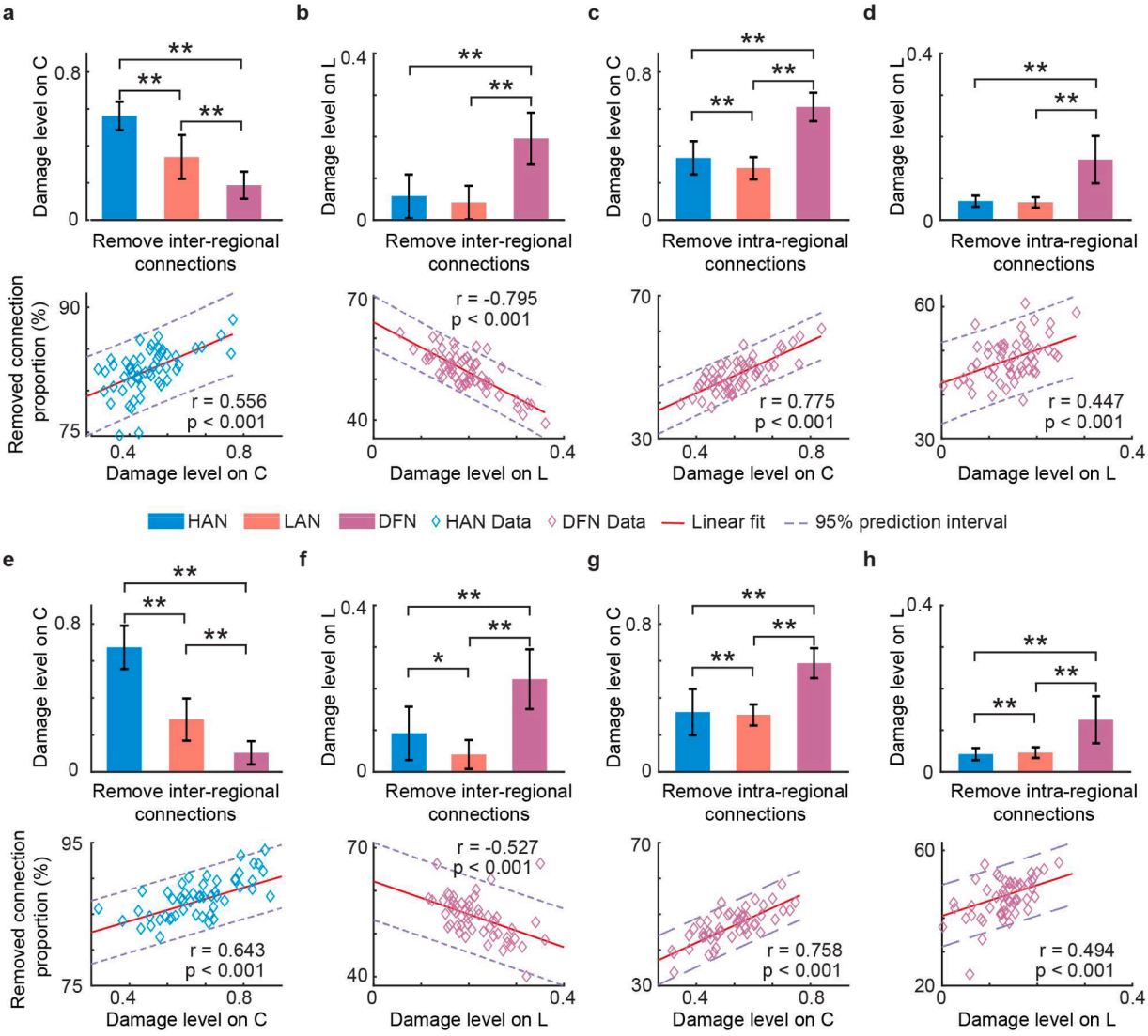

Fig. 5. Damages of (a) HAN, (b) LAN, and (c) DFN in ASD (Top panels) and COVID-19 (Bottom panels) under different types of attacks. Networks are selected from healthy controls of each dataset. The upper subplots show the damage levels of HAN, LAN, and DFN under corresponding damage types, such as removing inter- or intra-regional connections, while the lower subplots show the correlation between the damage level from the most damaged network and the proportion of connection be removed. **(a, b, e, f)** damages caused by removing inter-regional connections on *C* and *L*. **(c, d, g, h)** damages caused by removing inter-regional connections on *C* and *L*. These results indicate the high redundancy of the activation network connectivity pattern in the face of damage, and the DFN connectivity pattern is relatively fragile to both damage types. The activation network shows the importance of inter-regional connections, as evidenced by the positive correlation between the damage level on *C* and the proportion of inter-regional connections being removed. DFN shows the importance of intra-regional connections by the negative correlation between the damage level on *L* to the proportion of inter-regional connections being removed and by the positive correlation between the damage level on both *C* and *L* to the proportion of inter-regional connections being removed. **: $p < 0.001$, $FDR - corrected$.

Table 2
Graph properties of HAN, LAN, and DFN between patients and healthy controls.

		HAN			LAN			DFN		
		Patients	Healthy controls	*p*-value	Patients	Healthy controls	*p*-value	Patients	Healthy controls	*p*-value
ASD	*C*	0.536(0.190)	0.609(0.092)	**0.011**	0.317(0.094)	0.297(0.089)	0.261	0.464(0.031)	0.472(0.035)	0.230
	L	2.020(0.081)	1.989(0.055)	**0.020**	2.114(0.073)	2.126(0.058)	0.339	2.599(0.147)	2.555(0.109)	0.073
	El	0.677(0.165)	0.744(0.069)	**0.006**	0.478(0.081)	0.461(0.077)	0.268	0.652(0.034)	0.666(0.029)	**0.016**
	Eg	0.533(0.013)	0.538(0.009)	**0.013**	0.524(0.015)	0.521(0.011)	0.289	0.453(0.014)	0.456(0.013)	0.307
COVID-19	*C*	0.559(0.059)	0.569(0.065)	**0.043**	0.519(0.034)	0.516(0.045)	0.452	0.586(0.038)	0.589(0.036)	0.300
	L	1.754(0.006)	1.753(0.004)	**0.021**	1.795(0.019)	1.793(0.019)	0.103	1.898(0.075)	1.901(0.062)	0.689
	El	0.778(0.031)	0.783(0.034)	**0.037**	0.731(0.020)	0.727(0.026)	0.076	0.782(0.019)	0.782(0.017)	0.623
	Eg	0.624(0.001)	0.625(0.001)	**0.046**	0.621(0.005)	0.621(0.006)	**0.036**	0.602(0.011)	0.602(0.010)	0.621

Significant statistical differences ($p < 0.05$) are highlighted. Data are presented as mean(std).

3.6. HAN is more sensitive to mental state alteration than DFN

Towards real applications, graph theoretical analysis is applied to compare the performance of networks to reveal mental state alteration. HAN, LAN, and DFN of each participant are averaged along the time window and then used to calculate graph properties (clustering coefficient (*C*), characteristic path length (*L*), local efficiency (*El*), and global efficiency (*Eg*)). Table 2 compares the differences in graph properties between healthy controls and patients with ASD and COVID-19, respectively. For ASD, HAN shows a significant difference ($C: t_{108} = -2.572$, $p = 0.011$; $L: t_{108} = 2.359$, $p = 0.020$; $El: t_{108} = -2.799$, $p = 0.006$; $Eg: t_{108} = -2.513$, $p = 0.013$) in all graph properties between patients ($C: 0.536 \pm 0.190$; $L: 2.020 \pm 0.081$; $El: 0.677 \pm 0.165$; $Eg: 0.533 \pm 0.013$, *mean*±*std*) and healthy controls ($C: 0.609 \pm 0.092$; $L: 1.989 \pm 0.055$; $El: 0.744 \pm 0.069$; $Eg: 0.538 \pm 0.009$); DFN only shows a significant decrease ($t_{108} = -2.450$, $p = 0.016$) in *El* between patients (0.652 ± 0.034) and healthy controls (0.666 ± 0.029). For COVID-19, HAN still shows a significant difference ($C: t_{611} = -2.033$, $p = 0.043$; $L: t_{611} = 2.312$, $p = 0.021$; $El: t_{611} = -2.090$, $p = 0.037$; $Eg: t_{611} = -1.996$, $p = 0.046$) in all graph properties between patients ($C: 0.559 \pm 0.059$; $L: 1.754 \pm 0.006$; $El: 0.778 \pm 0.031$; $Eg: 0.624 \pm 0.001$)and healthy controls ($C: 0.569 \pm 0.065$; $L: 1.753 \pm 0.004$; $El: 0.783 \pm 0.034$; $Eg: 0.625 \pm 0.001$). However, there is no significant difference ($p > 0.05$) between patients and healthy controls using DFN. The theoretical graph analysis demonstrates that the topology of HAN is more related to brain mental state alteration and better at revealing the underlying dynamics of brain activity. Furthermore, results indicate a decrease in patients' brain information processing ability on global and local scales.

3.7. The activation network and DFN coordinate to provide more comprehensive information about the brain network

A data-driven method is applied to evaluate the practical applications of the activation network and DFN. We extract graph properties (*C*, *L*, *El*, *Eg*) within each time window as features used in feature selection and classification. For better comparison, we arrange features into three data groups according to network types: activation network (HAN and LAN), DFN, and a combination of the two networks. A data-driven feature selection method is applied to the training data to extract discriminative features of each group. Finally, these features are validated by various machine-learning classifiers (SVM, RF, Adaboost, NB). SVM with mixed features achieves the best classification accuracies (Table 3) in both datasets (ASD: 83.636 % ± 11.969 %; COVID-19: 67.333 % ± 5.398 %). The selected features effectively distinguish different mental states between patients and healthy controls. Notably, mixed features do not significantly increase classification accuracy when they do not add new, non-redundant information. The best classification performances are achieved by combining the activation network (AN) and dynamic functional network (DFN) features. We summarize all selected features across the 10-fold classification process. In the case of ASD, the HAN, LAN, and DFN contribute 25.641 %, 19.231 %, and 55.128 % of the total features (Supplementary Fig. 12), respectively. On the other hand, for COVID-19 classification, the HAN, LAN, and DFN contribute 58.108 %, 28.378 %, and 13.514 % of the total features (Supplementary Fig. 13), respectively. This result indicates that the activation network contains critical information representing other aspects of the brain communication process. Additionally, the DFN achieves the lowest classification accuracy, indicating the topology of the DFN is less sensitive to brain dynamics than the activation network. Combining the two networks provides a more comprehensive understanding of the brain network.

4. Discussion

This study proposed a new framework for segregating activity and background components in functional connectivity to distinguish FC's communication dynamic and non-dynamic dependencies. To capture the topological reorganization of the brain network, we propose the activation network as a spatiotemporal framework. We first validate the dynamic detection ability of AFC through simulation. The activation network is then applied to empirical datasets, revealing its advantage in extracting inter-regional connections between function-specific systems and establishing an efficient economic connectivity pattern that provides richer information about the reorganization of the network. Furthermore, both HAN and LAN are critical and play different roles in the activation network. HAN is particularly sensitive to changes in mental state, and when combined with LAN and DFN, they describe a more comprehensive picture of the communication process. Further detailed discussions are presented below.

BOLD-fMRI data are simulated using a combination of predefined temporal correlation and a first-order VAR model. We apply them to compose the background and dynamic components of correlation, respectively. Various models are used to generate dynamics of functional connectivity, such as large-scale dynamical models, neural field models, and neural network model (Demirtas et al., 2019; Honey et al., 2007). Since the underlying dynamics are unknown, the choice of model is arbitrary based on certain assumptions of physiological properties (Breakspear, 2017). Additionally, it varies according to the issue at

Table 3
Classification performances (%) of ASD and COVID-19.

		AN			DFN			MIXED		
		Sensitivity	Specificity	Accuracy	Sensitivity	Specificity	Accuracy	Sensitivity	Specificity	Accuracy
ASD	SVM	76.536 (19.149)	84.087 (12.236)	79.091 (11.379)	69.000 (18.760)	83.889 (17.656)	77.273 (7.726)	77.905 (25.166)	86.167 (19.052)	**83.636 (11.969)**
	RF	81.024 (17.601)	70.024 (18.387)	76.364 (10.671)	74.262 (22.922)	75.476 (18.009)	74.546 (18.581)	83.750 (17.174)	73.905 (28.607)	80.000 (20.009)
	AB	77.353 (31.601)	70.833 (26.932)	73.636 (23.648)	62.048 (22.847)	83.631 (15.305)	70.909 (15.920)	85.167 (16.744)	79.472 (20.423)	79.091 (12.159)
	NB	41.393 (23.253)	94.571 (8.878)	69.091 (10.671)	41.214 (24.769)	89.524 (13.756)	63.636 (12.856)	61.639 (23.775)	83.083 (21.531)	72.727 (18.182)
COVID-19	SVM	69.878 (8.702)	62.420 (8.335)	66.333 (5.317)	61.916 (8.822)	58.027 (8.809)	60.000 (3.685)	70.461 (8.644)	64.627 (8.469)	**67.333 (5.398)**
	RF	52.006 (13.091)	66.473 (8.876)	59.833 (5.355)	54.312 (11.861)	55.906 (15.348)	54.500 (7.073)	52.016 (12.886)	65.415 (8.291)	59.333 (5.731)
	AB	55.659 (9.327)	63.014 (8.414)	59.167 (3.948)	55.925 (10.445)	55.447 (10.771)	55.500 (5.614)	57.465 (10.048)	60.724 (11.347)	59.167 (4.321)
	NB	71.412 (25.554)	37.798 (25.328)	55.500 (3.518)	61.487 (18.879)	47.219 (19.284)	54.167 (4.462)	78.579 (7.232)	32.760 (9.118)	55.167 (6.500)

AN: activation network; DFN: dynamic functional network; MIXED: mixed features from both activation network and DFN; SVM: support vector machine; RF: random forest; AB: Adaboost; NB: naive bayes. The highest classification accuracy in each dataset is highlighted. Data are presented as mean(std).

hand. The current study is interested in the background and activity parts of functional connectivity. The experimental result indicates that predefined temporal correlation and the first-order VAR model are appropriate to simulate corresponding data in this study. Therefore, the selected simulation model is suitable for the current question.

The simulation results indicate that the calculated time-varying functional connectivity (FC) primarily reflects the background correlation trajectory, and the imputed dynamic data has minimal impact on the background correlation (Fig. 2a,b). The crucial question in practical applications is whether the non-dynamic dependency dominates functional connectivity. If detected BOLD-fMRI mainly reflects neural activity, the time-varying FC can efficiently capture the communication process, and any weak noise will not affect its dynamic detection ability. However, BOLD-fMRI signals are an indirect measure of brain activity and the neural dynamic is not the only property involved. Therefore, the calculated statistical correlation is constrained by the non-dynamic dependency of time series, and only a portion of its fluctuation is attributable to neural dynamics. This is supported by studies showing that the topography of BOLD-fMRI correlation still exists during slow-wave sleep and anaesthesia, where cognitive processes are absent or declined (Palanca et al., 2015; Mitra et al., 2015). Furthermore, patterns of FC are quite similar across the task-rest states, and over time (Li et al., 2020), indicating a predefined level of dependency within FC that is not sensitive to underlying neural fluctuations, and therefore cannot describe complex communication processes during brain activity. Consequently, FC is dominated by its non-dynamic dependency. These findings support the use of dynamic properties to evaluate connection rather than correlation strength. Simulation results from Fig. 2c,d show the ability of AFC to extract the ground truth of FC, indicating its reliability in modelling the dynamics of neural activity.

We applied the proposed method to two datasets (ASD and COVID-19). Notably, there are notable differences between the datasets: 1) participant populations: The ASD dataset comprises 100 children, while the COVID-19 dataset includes 613 adults; 2) data recording settings: The ASD data are recorded using an EPI sequence (TR 2 s, TE 30 ms, flip angle 90°, spatial resolution 3.4 * 3.4 * 3.0 mm) during a 10-minute eyes-open scan and COVID-19 data are recorded using an EPI sequence (TR 735 ms, TE 39 ms, flip angle 52°, spatial resolution 2.4 * 2.4 * 2.4 mm) during a 6-minute eyes-open scan. Despite the differences between the datasets, the experimental results of the activation network reveal similar spatiotemporal properties of healthy controls. This suggests that the activation network effectively captures the inherent properties of brain dynamics in diverse contexts, validating its robustness, reliability, and replicability. Heuristically, the differences between the two datasets suggest the activation network may explore age-related differences and the impact of recording settings on brain dynamics. Then, the experimental results of two datasets are discussed to reveal the performance of the activation network in the spatial and temporal domain.

The brain dynamic causes the complex reorganization of the brain network in the time dimension. In the experiments, DFN is hard to describe the reorganization processes due to the constrained network alteration in the time domain. This observation aligns with previous literature, highlighting the stable connectivity pattern during brain activity across various tasks and rest-task conditions (Finn et al., 2017; Gratton et al., 2016). Gratton et al. (Gratton et al., 2018) suggested that common organizational principles and individual features dominate the functional network. Rest-task and day-to-day variability are not the main factors in a functional network. However, extracting underlying temporal information is fundamental to a spatiotemporal network. It must be sensitive enough to describe the reconfiguration of the connectivity pattern during the communication process. From experimental results, the activation network exhibits richer network variations and different reorganization modes compared to DFN (Figs. 1d and 3). This suggests the potential of the activation network to extract dynamic of the brain activity. The reliability of the proposed method is further explored and validated in terms of the spatial and temporal properties of the activation network.

Network architecture helps us understand, predict and optimize the behavior of dynamic systems (Holme and Saramaki, 2012). We construct averaged spatial network of HAN, LAN, and DFN. From the results, they focus on the different communication modes. As shown in Fig. 4, DFN almost describes the outline of each functional system. Its connections are mainly located within the functional systems, showing significant intra-regional connections. For the activation network, it eliminates the constraint on the network reorganization and highlights the importance of inter-regional connection. Cole et al. (Cole et al., 2014) suggested cognitive tasks lead to complex changes from resting-state functional networks with increased multi-regional interactions and decreased within-network connectivity. Moreover, HAN and LAN are respectively associated with some function-specific subnetworks. HAN is more related to the inter-regional communications of SMN, while LAN is more related to the inter-regional communications of DMN. SMN is relatively more active in communicating with others. It is important to coordinate with CON in the function of sensory and behavior during the resting state and related to top-down control over the sensory region (Sadaghiani and D'Esposito, 2015; Crottaz-Herbette and Menon, 2006). Conversely, DMN appears to have significantly low activity during the resting state. This finding links previous results that DMN is not active with the functional demand of the human brain (Dosenbach et al., 2007; Singh and Fawcett, 2008).

We also need to validate whether the connectivity pattern of the activation network meets the basic requirements of most natural systems from the natural selection perspective. According to this theory, the dynamics of large-scale brain communication are expected to exhibit stability in communication efficiency and low wiring costs. From the aspect of wiring cost, as discussed in the simulation part, FC is not easily modified due to the strong impact of non-dynamic dependency. However, the AFC breaks this limitation isolating the dynamic dependency from FC, allowing for relatively free fluctuations. Cajal's law describes the optimization principles for conserving space, cytoplasm, and conduction time in neural circuitry (y Cajal, 1995). Based on the constrained network reorganization, optimization of operations on DFN cannot rebuild its connection from scratch for optimality (Avena-Koenigsberger et al., 2018). The activation network is not subject to this limitation, and the diversity of its connectivity pattern in the time domain also proves its low wiring cost. Furthermore, stable communication efficiency is another aspect of natural selection. C and L are applied to analyze the impact of lesion damage on communication ability at both global and local scales. The activation network demonstrates a higher redundancy of communication efficiency and emphasizes the significance of inter-regional connections. Its connectivity pattern is highly adaptable, enabling network reorganization during communication. In contrast, the DFN demonstrates the opposite behavior. These findings are in line with previous experimental results that have shown high spatial similarity in the connectivity pattern of DFN. The small-worldness of brain network topology is characterized by a balance between local segregation and global integration (Watts and Strogatz, 1998; Bassett and Bullmore, 2017; Cohen and D'Esposito, 2016; Wig, 2017), which is essential for maintaining optimal brain functioning. Redundant interactions during communication improve efficiency, robustness, and resilience to brain damage (Kaiser et al., 2007). Considering the low wiring cost of the activation network, the natural selection in network construction highlights the importance of the activation network in the time domain.

After exploring spatial and temporal activation properties, discussing the correlation between HAN and LAN is necessary. Even though both describe the activity of the brain network, the distributions of their graph parameters are different, indicating each network's unique reorganization process (Figs. 1d and 3). Moreover, the activation network exhibits stronger associations with specific function-specific subnetworks. HAN and LAN each highlight their respective functional

systems, leading to distinct information extracted by them. As a result, combining HAN and LAN composes a complete view of the activation network. The application of HAN and LAN depends on the aspect we want to analyze: dynamic communication between highly active functional systems or neural activity irrelative connectivity patterns during the communication process.

To apply the activation network to real-world scenarios, we assessed its reliability by utilizing graph properties to compare network topologies between healthy controls and patients. Our experimental results indicate that HAN reveals a marked contrast in network topologies between the two groups. In both ASD and COVID-19, HAN is the best to describe the decrement of brain processing ability (Table 2). The activation network is sensitive to mental state alteration. Furthermore, classification results also show the good performance of the activation network that the combination of features across HAN, LAN, and DFN acquires the best classification performance in both ASD and COVID-19. In particular, features from the activation network significantly improve the classification performance of the DFN. It not only suggests the reliability of the activation network but also indicates that both the activation network and DFN include critical and discriminative information about mental state alteration. In previous literature, a broad contribution of DFN demonstrated its capability in extracting cognitive contents (Rosenberg et al., 2016; Salehi et al., 2020). The activation network extends the contents of the brain network, making their combination better suited to reveal the properties of the brain network. Specifically, the DFN primarily characterizes the interactions among different brain regions, which may undergo minor changes during communication, leading to a relatively stable spatiotemporal connectivity pattern. On the other hand, the activation network focuses on the time-resolved activity of these interactions and is more sensitive to brain dynamics. The further applications of DFN and activation network depend on the specific research goals and objectives.

When interpreting our proposed activation network, certain aspects of the study require special consideration. Firstly, selecting a statistical method is the primary problem of activation network calculation. Numerous model-based and model-free computational methods exist for calculating directional or non-directional connectivity, such as mutual information, coherence analysis, transfer entropy, and others (Valdes--Sosa et al., 2011; Hassan and Wendling, 2018). In BOLD-fMRI studies, Pearson's correlation is the most frequently used method, with the linear correlation being the simplest way to combine time-invariant and time-specific properties of time series. Furthermore, the activity and background of functional connectivity is a general idea that could be applied to various statistical correlation methods. Integrating their time-invariant and time-specific features is a crucial challenge for using the activation network, particularly for nonlinear and directional correlation techniques, which is an area that requires further exploration. Secondly, the activation network does not describe the functional network but its activity in the time domain. Current dynamic brain network studies focused on the temporal alteration of the DFN based on statistical correlation. However, both the previous studies and experimental results in this paper indicate the limitation of DFN to extracting dynamic reorganization of the brain network. We extend a new view to establishing the brain network. The network construction is no longer limited to statistical correlations but also the non-correlation dependency within them. Thirdly, the proposed activation network is potentially applicable in EEG and fNIRS studies. Since EEG offers higher temporal resolution, it becomes particularly suitable for analyzing brain dynamics using the activation network. Our future work will apply and validate the proposed method, specifically in EEG-based mental tasks. Lastly, despite the good performance of the activation network, it is important to acknowledge its limitations. One notable area for improvement is its potential unsuitability for real-time analysis. This is primarily due to the requirement of utilizing the entire period data to obtain the time-invariant properties for calculating the BFC. Future research should also focus on addressing this problem.

5. Conclusion

This study proposes a spatiotemporal framework to describe the dynamic reorganization of the brain network. The temporal stability of DFN limits current studies. We apply AFC to extract dynamic fluctuation of statistical correlation and establish the activation network. Experimental results suggest that AFC shows a high correlation with underlying dynamics. Furthermore, the activation network spatially displays more multi-regional interactions with high sensitivity to mental state alteration. It temporally reveals more information about large-scale brain network communication with stable communication efficacy and low cost. The proposed method is validated by the application to achieve disorder classification. The activation network is an essential framework for understanding the brain network. Our research provides new insights into brain network construction and highlights the potential to employ the activation network in network neuroscience studies.

CRediT authorship contribution statement

Xucheng Liu: Conceptualization, Formal analysis, Investigation, Methodology, Validation, Visualization, Writing – original draft. **Ze Wang:** Conceptualization, Methodology. **Shun Liu:** Conceptualization, Methodology. **Lianggeng Gong:** Data curation, Resources. **Pedro A. Valdes Sosa:** Methodology, Writing – review & editing. **Benjamin Becker:** Methodology, Writing – review & editing. **Tzyy-Ping Jung:** Methodology, Writing – review & editing. **Xi-jian Dai:** Data curation, Resources, Project administration, Writing – review & editing. **Feng Wan:** Conceptualization, Supervision, Writing – review & editing, Funding acquisition.

Declaration of Competing Interest

The authors report no competing interests.

Data availability

The neuroimaging data are available from ABIDE (http://fcon_1000.projects.nitrc.org/indi/abide/) and UK Biobank (https://www.ukbiobank.ac.uk). The research data and code of this study are openly available in https://github.com/Xuchengliu/Activation-network-improves-spatiotemporal-modelling-of-human-brain-communication-processes.git.

Acknowledgements

This work was supported in part by The Science and Technology Development Fund, Macau SAR (File no. 0045/2019/AFJ, 0022/2021/APD, 0024/2023/ITP1 and 0024/2023/RIA1), The University of Macau Research Committee (MYRG projects 2017–00207-FST and 2022–00197-FST) and Guangdong Basic and Applied Basic Research Foundation (Grant No. 2023A1515010844). This research was conducted using the UK Biobank Resource under Application Number 94653 (PI: XI-jian DAI). This study was supported by Natural Science Foundation of Jiangxi Province (grant 20224BAB216077) and Hunan Province (grant 2022JJ40417 and 2021SK52203), incubation project of The Second Affiliated Hospital of Nanchang University for National Natural Science Foundation of China (grant 2022YNFY12008), and open funding from Key Laboratory of Medical Imaging and Artificial Intelligence of Hunan Province (YXZN2021003). Any opinions, findings, conclusions or recommendations expressed in this publication do not reflect the views of the Government of the Hong Kong Special Administrative Region or the Innovation and Technology Commission.

Supplementary materials

Supplementary material associated with this article can be found, in the online version, at doi:10.1016/j.neuroimage.2023.120472.

References

Amico, E., et al., 2017. Mapping the functional connectome traits of levels of consciousness. Neuroimage 148, 201–211.
Avena-Koenigsberger, A., Misic, B., Sporns, O., 2018. Communication dynamics in complex brain networks. Nat. Rev. Neurosci. 19, 17–33.
Barttfeld, P., et al., 2015. Signature of consciousness in the dynamics of resting-state brain activity. Proc. Natl. Acad. Sci. U.S.A. 112, 887–892.
Bassett, D.S., Bullmore, E.T., 2017. Small-world brain networks revisited. Neuroscientist 23, 499–516.
Breakspear, M., 2017. Dynamic models of large-scale brain activity. Nat. Neurosci. 20, 340–352.
Buckner, R.L., DiNicola, L.M., 2019. The brain's default network: updated anatomy, physiology and evolving insights. Nat. Rev. Neurosci. 20, 593–608.
Bullmore, E.T., Sporns, O., 2009. Complex brain networks: graph theoretical analysis of structural and functional systems. Nat. Rev. Neurosci. 10, 186–198.
Calhoun, V.D., Adali, T., 2016. Time-Varying Brain Connectivity in fMRI Data Whole-brain data-driven approaches for capturing and characterizing dynamic states. IEEE Signal Process. Mag. 33, 52–66.
Chang, C., Glover, G.H., 2010. Time-frequency dynamics of resting-state brain connectivity measured with fMRI. Neuroimage 50, 81–98.
Cohen, J.R., D'Esposito, M, 2016. The segregation and integration of distinct brain networks and their relationship to cognition. J. Neurosci. 36, 12083–12094.
Cole, M.W., et al., 2014. Intrinsic and task-evoked network architectures of the human brain. Neuron 83, 238–251.
Crottaz-Herbette, S., Menon, V., 2006. Where and when the anterior cingulate cortex modulates attentional response: combined fMRI and ERP evidence. J. Cogn. Neurosci. 18, 766–780.
De Luca, M., et al., 2006. fMRI resting-state networks define distinct modes of long-distance interactions in the human brain. Neuroimage 29, 1359–1367.
Demertzi, A., et al., 2019. Human consciousness is supported by dynamic complex patterns of brain signal coordination. Sci. Adv. 5, eaat7603.
Demirtas, M., et al., 2019. Hierarchical heterogeneity across human cortex shapes large-scale neural dynamics. Neuron 101, 1181–1194.
Di Martino, A., et al., 2014. The autism brain imaging data exchange: towards a large-scale evaluation of the intrinsic brain architecture in autism. Mol. Psychiatry 19, 659–667.
Dosenbach, N.U.F., et al., 2007. Distinct brain networks for adaptive and stable task control in humans. Proc. Natl. Acad. Sci. USA 104, 11073–11078.
Farahani, F.V., Karwowski, W., Lighthall, N.R., 2019. Application of graph theory for identifying connectivity patterns in human brain networks: a systematic review. Front. Neurosci. 13, 585.
Finn, E.S., et al., 2017. Can brain state be manipulated to emphasize individual differences in functional connectivity? Neuroimage 160, 140–151.
Fox, M.D., et al., 2005. The human brain is intrinsically organized into dynamic, anticorrelated functional networks. Proc. Natl. Acad. Sci. USA 102, 9673–9678.
Gratton, C., et al., 2016. Evidence for two independent factors that modify brain networks to meet task goals. Cell Rep. 17, 1276–1288.
Gratton, C., et al., 2018. Functional brain networks are dominated by stable group and individual factors, not cognitive or daily variation. Neuron 98, 439–452 e435.
Hassan, M., Wendling, F., 2018. Aiming for high resolution of brain networks in time and space Electroencephalography Source Connectivity. IEEE Signal Process. Mag. 35, 81–96.
Hermundstad, A.M., et al., 2013. Structural foundations of resting-state and task-based functional connectivity in the human brain. Proc. Natl. Acad. Sci. USA 110, 6169–6174.
Holme, P., Saramaki, J., 2012. Temporal networks. Phys. Rep. Rev. Section Phys. Lett. 519, 97–125.
Honey, C.J., et al., 2007. Network structure of cerebral cortex shapes functional connectivity on multiple time scales. Proc. Natl. Acad. Sci. USA 104, 10240–10245.
Honey, C.J., et al., 2009. Predicting human resting-state functional connectivity from structural connectivity. Proc. Natl. Acad. Sci. USA 106, 2035–2040.
Hutchison, R.M., et al., 2013. Dynamic functional connectivity: promise, issues, and interpretations. Neuroimage 80, 360–378.
Ji, J.L., et al., 2019. Mapping the human brain's cortical-subcortical functional network organization. Neuroimage 185, 35–57.
Kaiser, M., et al., 2007. Simulation of robustness against lesions of cortical networks. Eur. J. Neurosci. 25, 3185–3192.
Krienen, F.M., Yeo, B.T.T., Buckner, R.L., 2014. Reconfigurable task-dependent functional coupling modes cluster around a core functional architecture. Philos. Trans. R. Soc. B-Biol. Sci. 369, 20130526.
Laumann, T.O., et al., 2017. On the stability of BOLD fMRI correlations. Cereb. Cortex 27, 4719–4732.
Lewisa, C.M., et al., 2009. Learning sculpts the spontaneous activity of the resting human brain. Proc. Natl. Acad. Sci. USA 106, 17558–17563.
Li, L., Lu, B., Yan, C.G., 2020. Stability of dynamic functional architecture differs between brain networks and states. Neuroimage 216, 116230.
Liang, Z.F., Liu, X., Zhang, N.Y., 2015. Dynamic resting state functional connectivity in awake and anesthetized rodents. Neuroimage 104, 89–99.
Lu, J., et al., 2011. Focal pontine lesions provide evidence that intrinsic functional connectivity reflects polysynaptic anatomical pathways. J. Neurosci. 31, 15065–15071.
Lurie, D.J., et al., 2020. Questions and controversies in the study of time-varying functional connectivity in resting fMRI. Netw. Neurosci. 4, 30–69.
Mitra, A., et al., 2015. Propagated infra-slow intrinsic brain activity reorganizes across wake and slow wave sleep. eLife 4, e10781.
Mostame, P., Sadaghiani, S., 2021. Oscillation-based connectivity architecture is dominated by an intrinsic spatial organization, not cognitive state or frequency. J. Neurosci. 41, 179–192.
Mostame, P., et al., 2019. Statistical significance assessment of phase synchrony in the presence of background couplings: an ECoG study. Brain Topogr. 32, 882–896.
Palanca, B.A., et al., 2015. Resting-state functional magnetic resonance imaging correlates of sevoflurane-induced unconsciousness. Anesthesiology 123, 346–356.
Park, H.J., Friston, K., 2013. Structural and functional brain networks: from connections to cognition. Science 342, 1238411.
Petersen, S.E., Sporns, O., 2015. Brain networks and cognitive architectures. Neuron 88, 207–219.
Raut, R.V., et al., 2021. Global waves synchronize the brain's functional systems with fluctuating arousal. Sci. Adv. 7, eabf2709.
Ricchi, I., et al., 2022. Dynamics of functional network organization through graph mixture learning. Neuroimage 252, 119037.
Rosenberg, M.D., et al., 2016. A neuromarker of sustained attention from whole-brain functional connectivity. Nat. Neurosci. 19, 165–171.
Sadaghiani, S., D'Esposito, M, 2015. Functional characterization of the Cingulo-Opercular network in the maintenance of tonic alertness. Cereb. Cortex 25, 2763–2773.
Sakoglu, U., et al., 2010. A method for evaluating dynamic functional network connectivity and task-modulation: application to schizophrenia. Magnetic Resonance Materials in. Phys. Biol. Med. 23, 351–366.
Salehi, M., et al., 2020. There is no single functional atlas even for a single individual: functional parcel definitions change with task. Neuroimage 208, 116366.
Singh, K.D., Fawcett, I.P., 2008. Transient and linearly graded deactivation of the human default-mode network by a visual detection task. Neuroimage 41, 100–112.
Solé, R.V., et al., 2002. Selection, tinkering, and emergence in complex networks. Complex 8, 20–33.
Sporns, O., Betzel, R.F., 2016. Modular Brain Networks. Annu. Rev. Psychol. 67, 613–640.
Sudlow, C., et al., 2015. UK Biobank: an open access resource for identifying the causes of a wide range of complex diseases of middle and old age. PLoS Med. 12, e1001779.
Thompson, W.H., et al., 2018. Simulations to benchmark time-varying connectivity methods for fMRI. PLoS Comput. Biol. 14, e1006196.
Valdes-Sosa, P.A., et al., 2011. Effective connectivity: influence, causality and biophysical modeling. Neuroimage 58, 339–361.
Vidaurre, D., Smith, S.M., Woolrich, M.W., 2017. Brain network dynamics are hierarchically organized in time. Proc. Natl. Acad. Sci. USA 114, 12827–12832.
Vincent, J.L., et al., 2007. Intrinsic functional architecture in the anaesthetized monkey brain. Nature 447, 83–U84.
Wang, H.T., et al., 2021. Driving fatigue recognition with functional connectivity based on phase synchronization. IEEE Trans. Cogn. Dev. Syst. 13, 668–678.
Watts, D.J., Strogatz, S.H., 1998. Collective dynamics of 'small-world' networks. Nature 393, 440–442.
Wig, G.S., 2017. Segregated systems of human brain networks. Trends Cogn. Sci. (Regul. Ed.) 21, 981–996.
Xu, X.L., et al., 2021. Intrinsic connectivity of the prefrontal cortex and striato-limbic system respectively differentiate major depressive from generalized anxiety disorder. Neuropsychopharmacology 46, 791–798.
y Cajal, S.R., 1995. Histology of the Nervous System of Man and Vertebrates: General principles, Spinal cord, Spinal ganglia, Medulia & Pons. Oxford University Press.
Yang, X., et al., 2023. Age-dependent changes in the dynamic functional organization of the brain at rest: a cross-cultural replication approach. Cereb. Cortex. 33, 6394–6406. https://doi.org/10.1093/cercor/bhac512.
Zhang, J., et al., 2016. Neural, electrophysiological and anatomical basis of brain-network variability and its characteristic changes in mental disorders. Brain 139, 2307–2321.
Zhao, Z.Y., et al., 2019. Oxytocin differentially modulates specific dorsal and ventral striatal functional connections with frontal and cerebellar regions. Neuroimage 184, 781–789.
Zhou, T.Y., Kang, J.N., Cong, F.Y., Li, X.L., 2020. Early childhood developmental functional connectivity of autistic brains with non-negative matrix factorization. Neuroimage Clin. 26, 102251.
Zimmermann, K., et al., 2018. Altered orbitofrontal activity and dorsal striatal connectivity during emotion processing in dependent marijuana users after 28 days of abstinence. Psychopharmacology (Berl.) 235, 849–859.